

## Article

# Long Term Observation of Fractional Vegetation Cover in Qingyang of Gansu Province and Its Response to Climate Change

Jing Li <sup>1,2,3</sup> , Jianyun Zhang <sup>1,2,3</sup>, Xiaojun Wang <sup>1,2,3</sup>  and Guoqing Wang <sup>1,2,3,\*</sup> 

- <sup>1</sup> State Key Laboratory of Hydrology-Water Resources and Hydraulic Engineering, Nanjing Hydraulic Research Institute, Nanjing 210029, China; lij@nhri.cn (J.L.); jyzhang@nhri.cn (J.Z.); xjwang@nhri.cn (X.W.)  
<sup>2</sup> Yangtze Institute for Conservation and Development, Nanjing 210098, China  
<sup>3</sup> Research Center for Climate Change, Ministry of Water Resources, Nanjing 210029, China  
\* Correspondence: gqwang@nhri.cn

**Abstract:** Vegetation is seen as a sensitive indicator of global change because of its crucial role in connecting the atmosphere, soil, and water. Fractional vegetation cover (FVC), in turn, is an important indicator of vegetation status. Qingyang is a typically ecologically sensitive region, with a range of changes in vegetation in the last decade as a result of climatic and non-climatic factors. However, the exact impact of climate change and human activities remains unclear. Satellite observations can help to clarify that impact, allowing us to assess trends in vegetation change in the last two decades (2000–2019). In this study, daily and composite time series vegetation variations were derived from moderate resolution imaging spectroradiometer (MODIS) data and the impact of climate and human activity factors was examined for different administrative districts. By deploying multiple regression models, the research revealed that human activity has contributed 46% to the FVC variation, while the remaining 54% was led by climate factors. In areas where FVC was increasing, human activity contributed 55.89% while climate factors contributed 44.11%. In areas where FVC was decreasing, human activity and climate factors contributed 24.58% and 75.42%, respectively. The study also looks at the impacts of El Nino/IOD events in FVC dynamics in the study site. The FVC inversion result from MODIS proved capable of capturing long-term and seasonal vegetation patterns and thus provide a valuable archive for decadal-scale vegetation dynamics in the study area. Moreover, the improvement in FVC was a dual effect of climatic and human activities, while the latter owns a higher contribution especially for the implementation of ecological construction projects.

**Keywords:** vegetation; climate change; human impact; Qingyang



**Citation:** Li, J.; Zhang, J.; Wang, X.; Wang, G. Long Term Observation of Fractional Vegetation Cover in Qingyang of Gansu Province and Its Response to Climate Change. *Atmosphere* **2022**, *13*, 288. <https://doi.org/10.3390/atmos13020288>

Academic Editor: Alfredo Rocha

Received: 17 January 2022

Accepted: 5 February 2022

Published: 8 February 2022

**Publisher's Note:** MDPI stays neutral with regard to jurisdictional claims in published maps and institutional affiliations.



**Copyright:** © 2022 by the authors. Licensee MDPI, Basel, Switzerland. This article is an open access article distributed under the terms and conditions of the Creative Commons Attribution (CC BY) license (<https://creativecommons.org/licenses/by/4.0/>).

## 1. Introduction

Land use/land cover change (LUCC) is one of the core components of global change research. Land cover plays an essential role in terrestrial life support systems and serves as an important monitoring indicator to reflect the state of the regional ecological environment [1,2]. Moreover, as the link between different layers of the earth system, it also has a great influence on the components of those layers. Land use is one of the direct ways human activities act on the natural environment and is also the most direct and leading driving factors of land cover change throughout history [3,4]. LUCC is generally regarded as the most obvious phenomenon of global changes and will have a great effect on terrestrial ecosystems and functions in the next 30 to 40 years, and closely related to the humanistic process [5].

Vegetation is considered the most important component of terrestrial ecosystems but is also highly sensitive to climate change. Fractional vegetation cover (FVC) is commonly regarded as the fraction of green vegetation seen from the nadir of the total statistical area [6–8]. Long-term observation of surface vegetation cover and its variation can have

great practical significance. It can reflect trends in climate change to a certain degree while also indicating surface space change, the forces behind that change, and the condition of the regional ecosystem [9,10]. This is in large part why analysis of the relationship between vegetation variation and climate change has become a focus of research worldwide.

The inseparable relationship between climate change and vegetation is mainly manifested in two ways: the adaptability of vegetation to climate and the feedback effect of vegetation on climate. Climate is the most important factor that determines the type and distribution of vegetation, while vegetation is the most distinctive and comprehensive reflector of climate. However, as economies expand rapidly and human activities intensify, the global climate is undergoing significant changes. Overconsumption of natural resources, accelerating urbanization, and the discharge of large amounts of CO<sub>2</sub>, and other greenhouse gases into the atmosphere, have led to a series of serious issues, including rising temperatures and environmental pollution [11,12]. The severe consequences pose threats to ecosystems, societies, infrastructures, and industry, as well as national interests and security. Therefore, global changes, in combination with other anthropogenic stressors will induce vegetation types and coverage to a regional and global extent [13–15]. The scale of influence is expanding and a clear manifestation at the regional scale has been observed and verified. Given that the global climate may further warm, it is crucial to explore the variation trend of regional climate-related factors. Many researchers have shown that vegetation cover variation is a consequence of the dual effects of climate change and anthropogenic activities. At the same time, vegetation variation can show the influence of human activities to a certain extent. Despite several studies focused on the assessment of vegetation dynamics at different locations or time scales, the quantitative relationship between vegetation variation and climatic factors and human activities remains to be fully assessed [14,16,17]. It is noteworthy to explore the related driving factors of vegetation growth and to which extent the vegetation dynamic has been influenced by climatic and anthropogenic factors, respectively.

The Loess Plateau has been a focus of national efforts to foster the environment and introduce sustainable development. It is well-known in the world due to serious soil erosion. The Loess Plateau is also fragile in the ecological environment because of its sensitivity to climate change [18]. The area has been subjected to poor use of land resources driven by relatively backward socio-economic and traditional inefficient agro-pastoral economic development patterns. Expansion in the heavy industry further aggravated the destruction of natural resources and resulted in severe environmental pollution.

Within that area, Qingyang is rich in resources ecologically fragile. It has a wealth of oil, coal, and natural gas and is growing rapidly with the development of those industries over the last decades. This has enabled high-speed growth in the local economy, as well as undeniable negative effects, such as pollution and destruction of the ecosystem.

Those changes are reflected in FVC variation, which can be assessed using a combination of remote sensing, GIS, and other techniques. Furthermore, several large-scale FVC products have been created based on different sensors, including SPOT VGT, MERIS, AVHRR using different estimation methods [19–23]. These long-term and reliable observations can help us better understand how to explore and utilize climate resources and land resources rationally, find pathways to protect the ecosystem, and further effectively promote the sustainable development of society and those resources.

In our research, we derived the long-term record of FVC in Qingyang using MODIS images, looking at the temporal and spatial distribution characteristics of FVC. With the help of meteorological inversion data, the relationship between FVC and climatic factors was analyzed. Furthermore, the contribution of climate change and human activities to vegetation variation was quantified. Our research could provide spatial information support for the assessment of Loess Plateau ecosystem change, and analytical support for environmental monitoring programs.

## 2. Materials and Methods

### 2.1. Study Site

Qingyang is a provincial city in the eastern part of Gansu Province (Figure 1). It borders Shaanxi province and Ningxia Hui autonomous region and covers 27,119 km<sup>2</sup> [24]. Qingyang administers Huan, Huachi, Qingcheng, Heshui, Ning, Zhengning, and Zhengyuan counties and Xifeng. It is also a typical example of a rapidly growing mid-size city in north-west China. The city is rich in oil, gas, coal, and other mineral resources and the main industries are oil production, refining, and transportation, which contribute 11.5%, 50.1%, and 38.4%, respectively to the local economy. In 2019, Qingyang had a total population of 2.28 million and a GDP of 74.29 billion yuan.

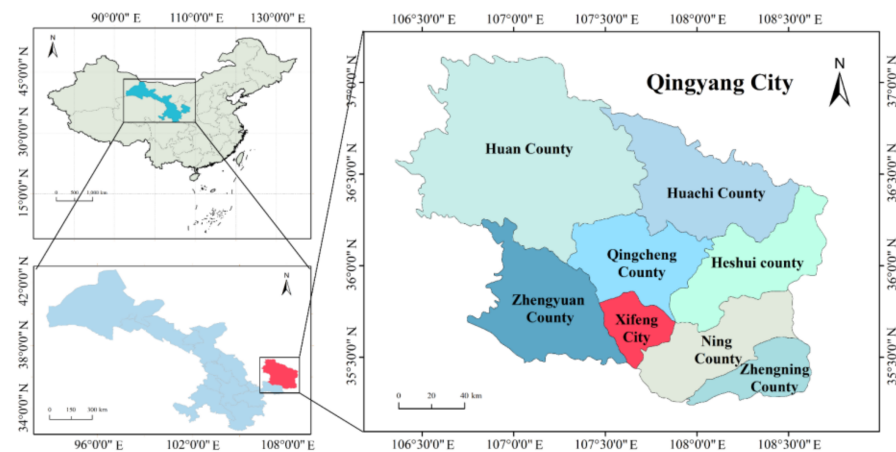


**Figure 1.** Location of the Qingyang city in Gansu Province, China.

In recent decades, the city has undergone rapid urbanization and industrialization [25]. It is also ecologically vulnerable to extreme environmental changes as a result of climate change and low vegetation cover [26].

### 2.2. Data Sources

The 250-m moderate-resolution imaging spectro-radiometer (MODIS) grid was downloaded for the year 2000–2019 from NASA. The MOD09 and MYD09 products were deployed. Daily red and near-infrared (NIR) surface reflectance was acquired from the product with a spatial resolution of 250 m in Hierarchical Data Format (HDF). Daily quality assessment (QA) flags were used to collect to identify the state of atmosphere and acquisition position (e.g., presence of clouds, cirrus, aerosol concentration). The 6S radiative transfer model was processed for atmospheric correction to obtain the surface reflectance [27]. Data preparation was conducted in three steps. First, cloud removal was conducted by visual interpretation. Second, time series was conducted to refill the introduced gaps. Third, monthly aggregation was calculated.

The GPM Core Observatory was launched as the TRMM successor in February 2014 in a collaboration between the National Aeronautics and Space Administration (NASA) and the Japan Aerospace Exploration Agency (JAXA). It provides global rain and snow observations with a spatial resolution of  $0.1^\circ \times 0.1^\circ$  and a temporal resolution of half-hourly [28]. Our study focused on the daily final product of level 3 IMERG (integrated multi-satellite retrievals for GPM) data at a spatial resolution of  $0.1^\circ \times 0.1^\circ$ . The data can be accessed from NASA (<https://disc.gsfc.nasa.gov/datasets?keywords=GPM&page=1>, accessed on 6 June 2021).

The ERA-Interim reanalysis data was deployed in our research. The ERA-Interim reanalysis dataset is produced by the European Center for Medium-Range Weather Forecasts (ECMWF). It contains the latest global atmospheric product in multiple spatial and temporal resolutions. We used the monthly temperature data at four time periods (UTC 00:00,

06:00, 12:00, 18:00) with a spatial resolution of 0.125 degrees. Bilinear interpolation was used to resample the ERA-Interim data to match the spatial resolution of MODIS images.

In order to analyze the impact of human activity on vegetation variation, data on population (containing the total, rural and urban population) and gross domestic product (GDP) were also factored into the analysis. These data were collected from the statistical yearbooks published by the local government.

### 2.3. Methodology

#### 2.3.1. FVC Calculation

The NDVI is one of the most accepted parameters in the ecological studies [29–31]. It can be expressed as [32]

$$\text{NDVI} = (r_{\text{nir}} - r_{\text{r}}) / (r_{\text{nir}} + r_{\text{r}}) \quad (1)$$

where  $r_{\text{nir}}$  and  $r_{\text{r}}$  stand for the surface reflectance in the near-infrared and red spectral range, respectively. NDVI value ranges from  $-1$  to  $1$  [33].

In this study, the dimidiate pixel model was used to calculate the FVC for the study site and based on assumption that the ground object information only consisted of mixed pixels of vegetation and soil information [34,35]. The NDVI value can be expressed as

$$\text{NDVI} = \text{FVC} \times \text{NDVI}_{\text{veg}} + (1 - \text{FVC}) \times \text{NDVI}_{\text{soil}} \quad (2)$$

where  $\text{NDVI}_{\text{veg}}$  stands for the NDVI value for vegetation only of the mixed pixel, while  $\text{NDVI}_{\text{soil}}$  is the NDVI value of the pure soil part of the mixed pixel. Then, the FVC can be calculated from the following formula:

$$\text{FVC} = (\text{NDVI}_i - \text{NDVI}_{\text{soil}}) / (\text{NDVI}_{\text{veg}} - \text{NDVI}_{\text{soil}}) \quad (3)$$

where  $\text{NDVI}_i$  is the NDVI value of the selected pixel. Due to the influences from various factors, such as atmosphere and vegetation phenology, the value of  $\text{NDVI}_{\text{veg}}$ ,  $\text{NDVI}_{\text{soil}}$  cannot be fixed [36,37]. We have considered using the MODIS land cover product (MOD12Q1) to retrieve the vegetation type for the study site. However, MOD12Q1 only has two values in Qingyang city, which is too coarse to determine the specific vegetation type. Therefore, in our research,  $\text{NDVI}_{\text{veg}}$  is determined by the 95% quantile of the highest value of NDVI from each scene during summer for each year. In our research,  $\text{NDVI}_{\text{veg}}$  is determined by from the 95% quantile of the highest value of NDVI from each scene during summer for each year.  $\text{NDVI}_{\text{veg}}$  is taken as the 5% quantile of the lowest value of each scene of all images in the calculation for the whole year.

#### 2.3.2. Temporal Decomposition

The Census X-11 method was used to calculate a temporal decomposition of monthly FVC for each pixel [38,39]. This is an iterative algorithm using simple moving averages. The method decomposed the time series  $X(t)$  into three additive components ( $S(t)$ ,  $T(t)$ ,  $I(t)$ ), which can be expressed as

$$X(t) = S(t) + T(t) + I(t) \quad (4)$$

where  $S$  stands for the seasonal component,  $T$  refers to the trend component, and  $I$  means irregular component.

The bandpass-filtering methods were based on the utilization of successive filters, containing a simple moving average, seasonal moving average, and Henderson filter [40]. Every component is calculated with an iterative procedure with an alternate computation of the trend component from seasonally adjusted records, and the seasonal component from the corrected trend series [41,42].

#### 2.3.3. Seasonality Analysis

We also compared information on regional FVC seasonality in different periods, with the first period from 2000 to 2002 and the latter from 2003 to 2019. Using the approach

suggested by Chan and Ripley [43], harmonic functions were first applied from each pixel time series. Then the changes in seasonal phase and amplitude ( $\Delta\text{FVC}$ ) were estimated based on peak vegetation activity through the year. The seasonal phase shifts were calculated from the subtraction between the month in which  $\text{FVC}_{\text{max}}$  occurred during 2003–2019 and the referring month during 2000–2002. Accordingly,  $\Delta\text{FVC}_{\text{max}}$  was calculated as the subtraction from two corresponding values of  $\text{FVC}_{\text{max}}$ .

#### 2.3.4. Multiple Linear Regression (MLR) Models

The vegetation variation is influenced both by climate variables such as changes in temperature and precipitation, and human activities which can both be positive and negative. The human variables include human internal migrations, overgrazing [44], ecological restoration projects leading to afforestation, and returning farmland [45,46]. We used MLR modeling to separate the influence of climate and human activities on vegetation variation. For each pixel, we assume the variation in FVC is due to three factors: climate variables, non-climate variables (regarded as human impacts), and random error (which should be normally distributed with a mean value of zero). We assumed that the random errors had no trend. Therefore, the trends identified in residuals were attributed to human activities. Climate factors (temperature and precipitation) were set as the independent variable while the FVC was treated as a dependent variable. Then the predicted FVC ( $\text{FVC}_{\text{pre}}$ ) was calculated as,

$$\text{FVC}_{\text{pre}} = A \times T + B \times P + C \quad (5)$$

where T and P stand for monthly average value of temperature and precipitation, A, B, and C were regression coefficients. The residual FVC ( $\text{FVC}_{\text{res}}$ ) can be expressed as,

$$\text{FVC}_{\text{res}} = \text{FVC}_{\text{obs}} - \text{FVC}_{\text{pre}} \quad (6)$$

where  $\text{FVC}_{\text{obs}}$  stands for the inversion result, the residual stands for the FVC value influenced by human activities and the prediction FVC value means the value dominated by climate factors. Similar methods have been implemented in previous studies such as Wessels et al. [47] and Chun et al. [48].

### 3. Results and Discussion

#### 3.1. Spatial Pattern of Monthly FVC Variation

The spatial distribution of FVC monthly variation indicates strong periodicity (Figure 2). In general, the southeast part has the highest FVC while the northeast has the lowest value of the whole area over the year. Higher variations of FVC were observed in the southeast, followed by the central part and northwest. The greening trend was first observed in March from the southeast. Gradually, the area of high vegetation increased and moved northwest. The largest coverage area of high FVC was in July and August. During this period, the FVC value for the southeast part of Qingyang was higher than 0.6, the central part was higher than 0.4, the most northern part was around 0.2. The least variation value between these three regions was observed over the year. A browning trend was observed from September and gradually moved from the northwest to the southeast.

Vegetation has a certain growing circle and regularity. In the Loess Plateau in China, the vegetation turns green in spring and grows most luxuriant in summer, and leaves begin to fall in autumn. This cyclical change was well reflected in the time series observation (Figure 3). The FVC value presented a significant increase from April and peaked in August, declining to 0.2 in December. There was no obvious variation trend from January to March, where there was the lowest FVC value of the year. The same trends were observed in each administrative district.

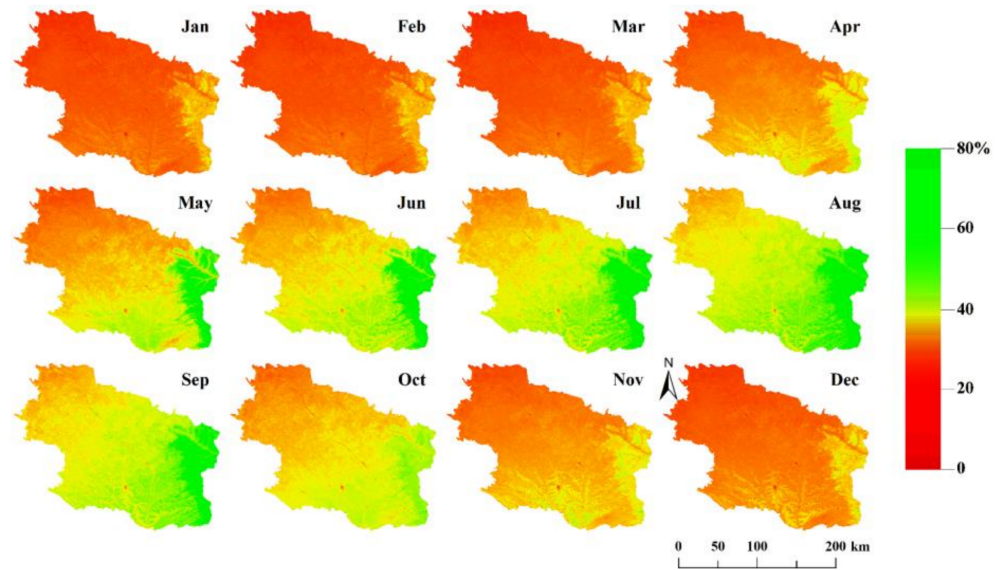


Figure 2. Spatial distribution of FVC monthly variation in Qingyang.

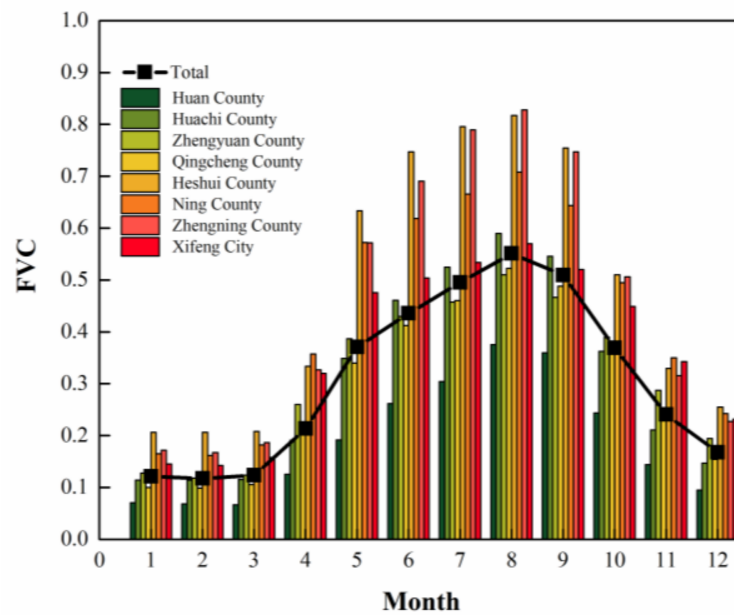
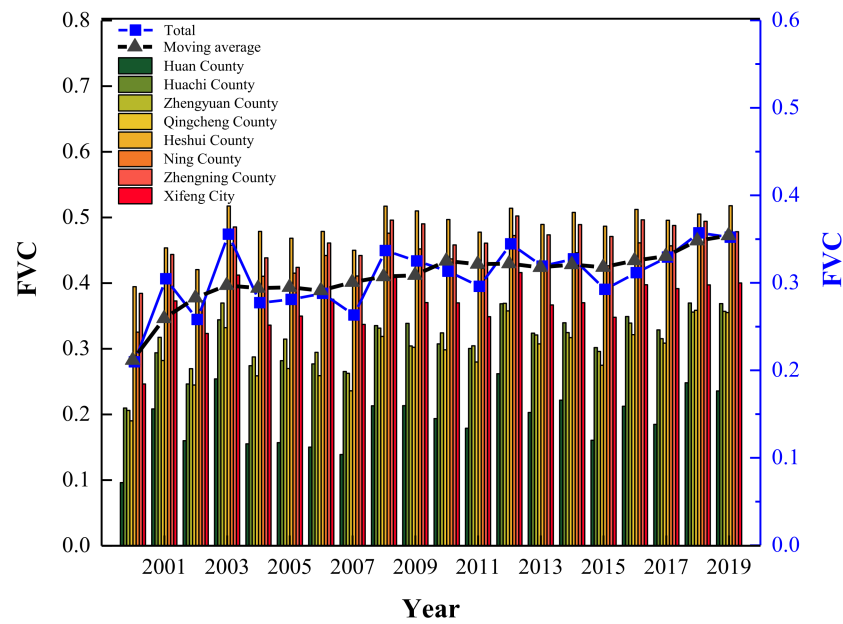


Figure 3. Seasonal pattern of FVC in Qingyang.

### 3.2. Variation of Annual FVC and Its Spatial Pattern

The annual records of FVC for Qingyang showed a significant increase from 2000 to 2019 with an average value of 30.71%. The minimum FVC of 20.97% was in 2000 while the maximum of 35.71% was in 2018. In general, the five-year moving average showed an increasing trend from 2000 to 2010 for the Qingyang area. A significant increasing trend was found from 2000 to 2003, 2009 to 2010, and 2015 to 2020. Smooth changes were found from 2003 to 2006, 2010 to 2015. Similar, trends were observed in each administrative district (Figure 4).



**Figure 4.** Annual records of FVC in Qingyang from 2000 to 2019.

The spatial distribution of average FVC for the whole year around and growing season were obtained using long-term series monthly mean FVC images (Figure 5). Latitude zonality of FVC distribution was found on both annual and growing season records, with the FVC value increasing from the northwest to the southeast. Higher FVC was found during the growing season in almost every part of Qingyang.

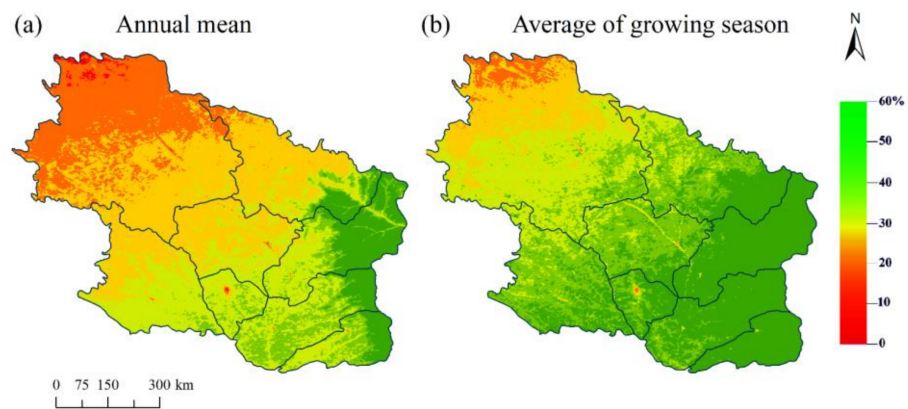


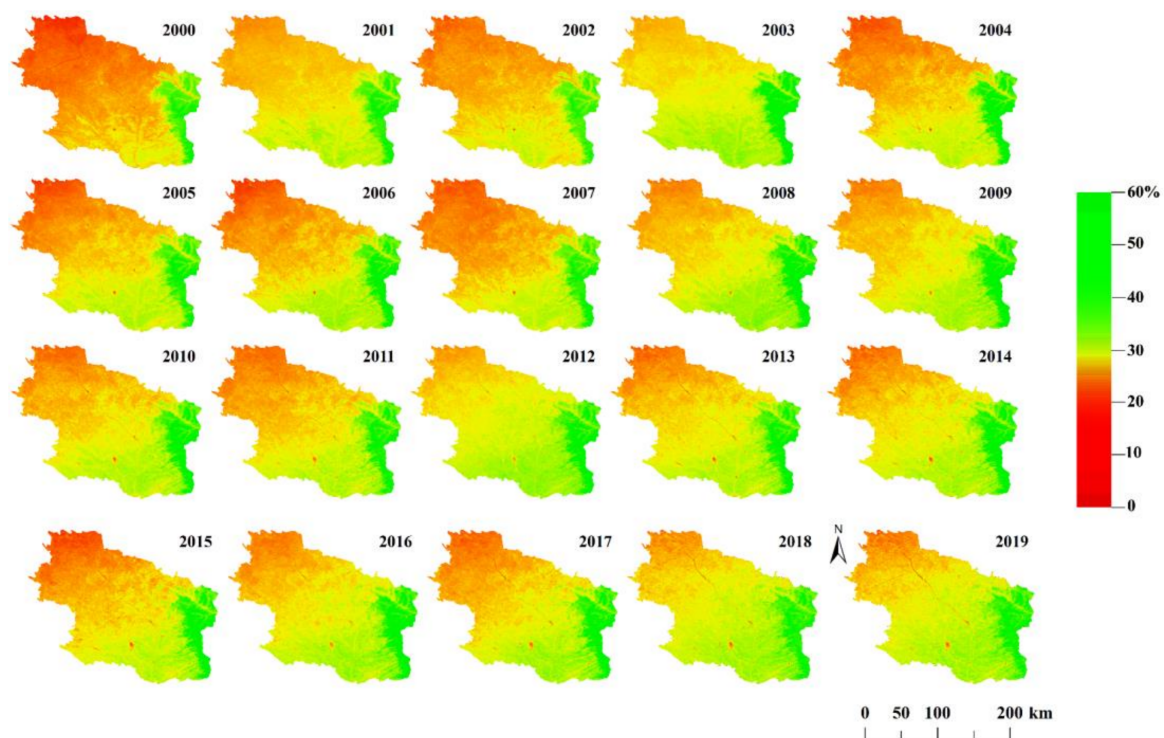
**Figure 5.** Spatial distribution of historical FVC average value for (a) annual (b) growing season from 2000 to 2019.

The percentage of covered area for different FVC range at annual and season periods was listed in Table 1. The lowest average FVC was observed in the north of Huan county both in the annual and growing season. Especially for FVC under 20%, it covers 19.95 and 2.48% of the whole area, respectively. Large differences between annual and growing seasons in FVC were at the range of 40 to 60%, with covering areas of 14.23% and 39.14%, respectively. The variation is mainly distributed in Huachi, Qingchen, Zhenyuan counties, and Xifeng. High FVC with a value of more than 60% amounted to 23.86% of the whole area, which is about seven times the annual result and was detected mainly in Heshui, Zhengning, and Ning counties.

**Table 1.** Percentage of coverage area for different FVC for annual and growing season mean.

FVC	Annual	Growing Season
<10%	0.62	0.00
10–20%	19.33	2.48
20–30%	34.87	11.85
30–40%	26.10	22.66
40–50%	9.15	25.27
50–60%	5.08	13.87
>60%	4.85	23.86

The annually spatial variations of vegetation trends are shown in Figure 6. The data showed a similar spatial distribution pattern with the higher FVC in the southeast and the lower FVC in the north. The greening trend was clearly revealed over the 20 years of the record. In 2000, 82.28% of the area had an FVC lower than 0.3 with a coverage area of 22,314.73 km<sup>2</sup>. A remarkable improvement was observed from 2003. Just 11,018.7 km<sup>2</sup> had an FVC < 0.3, less than half the area observed for 2000. By 2019, the area with FVC < 0.3 decreased to 9545.98 km<sup>2</sup> or 35.20% of the whole area. At the same time, the area with FVC > 0.6 increased from 268.92 km<sup>2</sup> in 2000 to 1236.45 km<sup>2</sup> in 2019, the difference of 967.53 km<sup>2</sup>.

**Figure 6.** Annually spatial variation records of Qingyang from 2000 to 2019.

The linear regression slope and significant value of  $\tau$  are shown in Figure 7. A similar spatial trend was obtained from both coefficients. For the slope coefficient, 96.71% of pixels showed a positive trend while 3.29% were negative. For Kendall's  $\tau$  coefficient, 95.63% of the grids were positive and 4.37% were negative. Browning mainly occurred in the southeast part of Zhengyuan and Zhengning counties. Negative trends were also observable in distinct locations along the north boundary of Huan county.

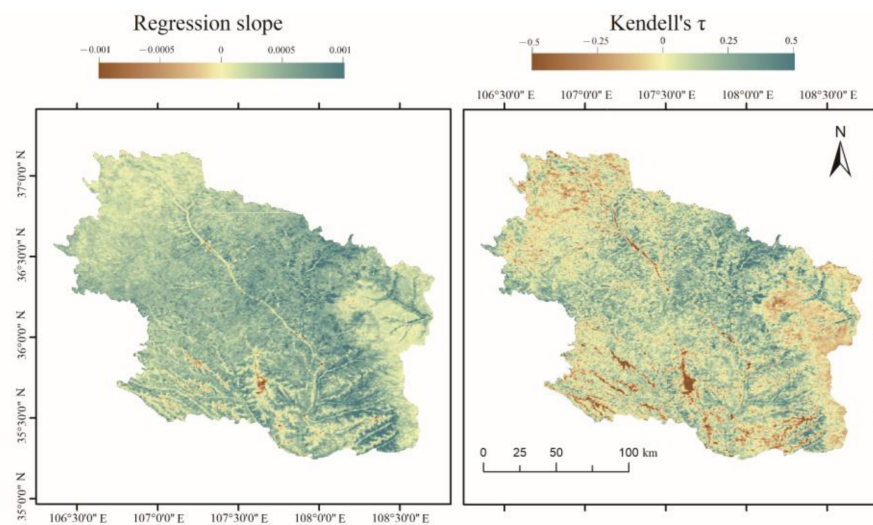


**Figure 7.** Linear regression slope and Kendall’s  $\tau$  ( $p < 0.001$ ) derived from monthly FVC between 2000 to 2019.

### 3.3. Temporal Decomposition of FVC

The Census X-11 method was applied to monthly FVC and the decomposition result is shown in Figure 8. Five trend breakpoints were observed around July 2002, July 2003, August 2008, March 2012, and March 2018. A rapid decrease was found in 2003 while a significant increasing trend was observed around the other four breakpoints. No seasonal breakpoints were identified. In addition, multiple sudden upward shifts interrupting the downward trend were found during 2012–2013 and 2015–2016.

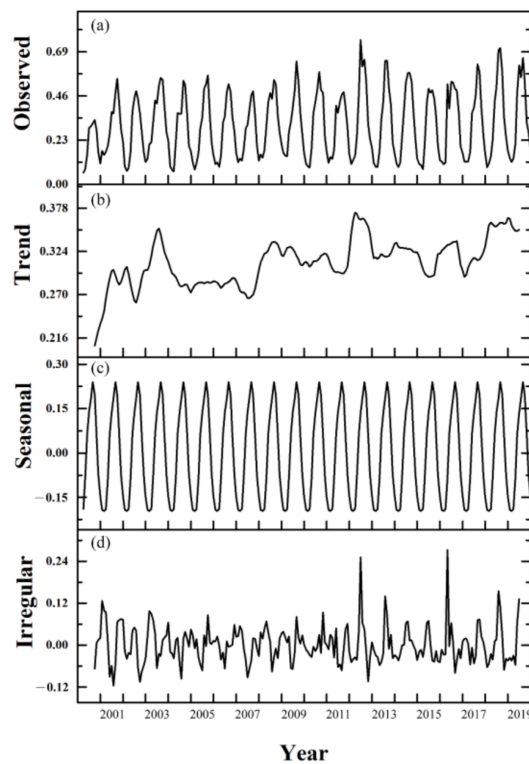


**Figure 8.** Decomposition result of FVC variation from 2000 to 2019 in Qingyang including (a) input time series, (b) trend component, (c) seasonal cycle, and (d) irregular signal.

From a temporal perspective, the month during which  $FVC_{max}$  was found followed a northwest to southeast gradient. From 2000 to 2002, there was an earlier onset in the south and later onset in the northeast during the year. For the 2003–2019 period, there was a variation in the onset, and most of the area had an earlier onset compared to the previous time. Several discrete points in the eastern part of Huan county had a forward onset compared to the surrounding areas.

Forward and backward shifts of the peak month are shown in Figure 9c. Overall, negative shifts in the pixels were much higher than positive shifts. Positive (+) shifts were mainly in the southwest corner of Qingyang, covering Ning and Zhengning counties, and Xinfeng. Negative (−) shifts dominated most of Huan county and the eastern part of Qingyang, including the eastern areas of Heshui, Ning and Zhengning counties.

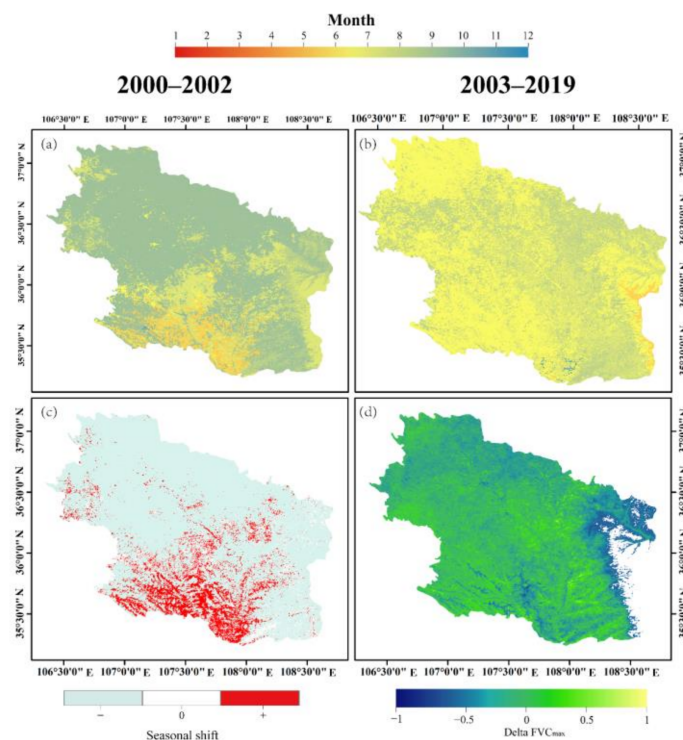


**Figure 9.** (a) Month with maximum vegetation activity derived from peak FVC from 2000–2002 and (b) 2003–2019. (c) Estimating seasonal phase shift (‘−’ dedicates an earlier while ‘+’ means a later occurrence of  $FVC_{max}$ , and (d) seasonal amplitude change of  $FVC_{max}$ .

Seasonal amplitude changes were calculated (Figure 9d), reflecting increasing greenness across the whole area. An area in the east Ziwuling forest was blank because there were no seasonal amplitude changes in this area. Our results indicate that the  $\Delta FVC$  corresponded well with the spatial patterns of the monotonic greening and browning shown in Figure 7.

### 3.4. Quantifying the Contribution from Climate Factors and Human Activities

The long-term variation trend of FVC in Qingyang is shown in Figure 10a. Of the whole area, 95.43% demonstrated a positive trend, with most staying around  $3 \times 10^{-3}/a$  to  $5 \times 10^{-3}/a$ , covering 63.63% spatial area. The trend of  $2 \times 10^{-3}/a$  to  $3 \times 10^{-3}/a$  and 0 to  $1.5 \times 10^{-3}/a$  followed, covering 13.33% and 12.65%, respectively. The area with a negative trend occupied 4.57% of the whole area.

We used the MLR models to determine the FVC trends dominated by climate variables and human impacts (Figure 10). On the condition of climate variables dominated, the comparative result of FVC variation were demonstrated in Figure 10b. Over the entire Qingyang region, 98.73% of the grids displayed a positive trend, with 57.63% located at 0 to  $2 \times 10^{-3}/a$ , and the coverage area increased by 39.15% compared to the FVC trend

in Figure 10a. The increasing area is mainly located in the northern part of Huan county, eastern part of Huachi, Heshui and Zhengning counties, as well as the southwest part of Ning county and the central part of Xifeng. The grids ranging from  $2$  to  $3 \times 10^{-3}/a$  increased 21.63%, covering the southwest part of Huan county and Huachi county, and the northern part of Heshui county. The grids in the range of  $3$  to  $5 \times 10^{-3}/a$  decreased by 57.48%. The decreasing trend mainly covered the southern part of Huan and Huachi counties, and most of Zhengyuan, Qingcheng, Ning counties, and Xifeng.

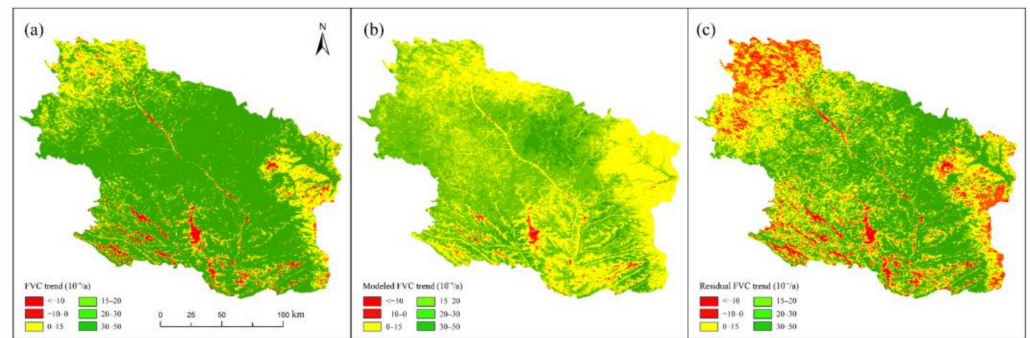


**Figure 10.** Trend variation of FVC in Qingyang from 2000 to 2019. (a) FVC trend; (b) dominated by climate variables; (c) dominated by human factors.

The spatial distribution of human variables that impacted the FVC trend are shown in Figure 10c. In all, 85.44% of the grids demonstrated a positive trend, with a decrease of 13.29% comparing to climate variable dominated conditions. The decrease was mainly in the range of  $1.5$  to  $3 \times 10^{-3}/a$ . In contrast, a large increasing trend was discovered from  $3$  to  $5 \times 10^{-3}/a$ , with the area increasing by 25.76%, covering the southwest part of Heshui county, the central part of Ning county, and in Zhenning county. A total of 14.56% of the grids demonstrated a decreasing trend, and these were in the northwest of Huan county and southeast part of Heshui county.

The contributions of climate and human factors to long-term FVC variation (2000–2019) are shown in Figure 11. In general, the FVC variation is affected by both climate and human factors, with each contributing 54% and 46%, respectively.

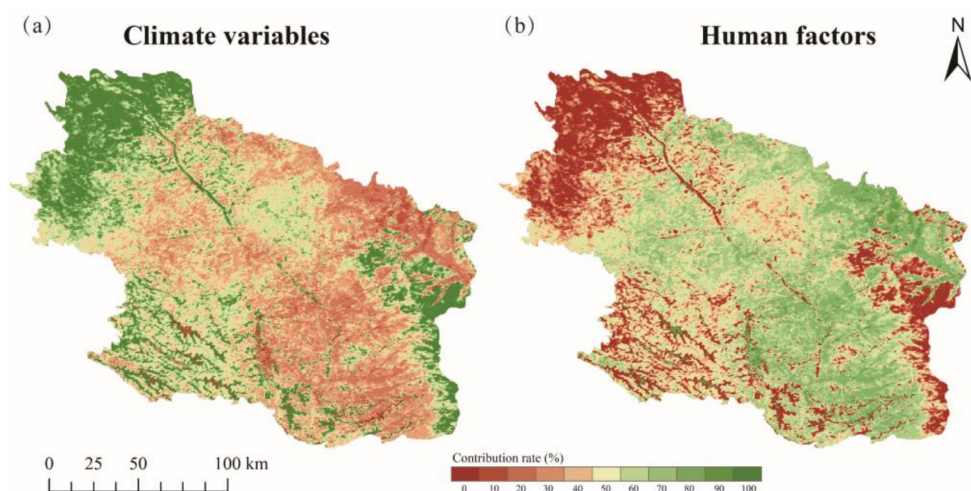


**Figure 11.** Contribution of (a) climate variables and (b) human factors.

On a spatial scale, the area with a positive FVC trend was highly influenced by human activities, with 55.89% of the increasing grids dominated by human activities (with the contribution rate  $>50\%$ ) and 12.08% of the area with a contribution rate of human activities

higher than 70%. Human activities most influenced the eastern part of Huachi county, the western part of Heshui county, and the central part of Ning county. The contribution rate ranges from 50 to 70% in most of central Qingyang.

In total, 44.11% of the area with an increasing FVC trend was influenced by climate factors and was found in the northeast part of Huan and Zhengyuan counties, the western part of Huachi county, and the easternmost part of Heshui, Ning, and Zhengning counties. The northeast part of Huan county and the easternmost part of Heshui, Ning and Zhengning counties were highly influenced by climate factors (with the contribution rate higher 70%), accounting for 21.88% of Qingyang.

Climate factors dominated the negative FVC trend covering 75.42% of the decreasing FVC grids. High influences (with a contribution of more than 70%) were detected in the western part of Zhengyuan and Ning counties, the eastern part of Heshui county and in Zhengning county, covering 74.82% of the area.

The remaining 24.58% of the decreasing FVC trend was affected by human activities, and mostly found in the central part of Zhengyuan county (with the contribution rate higher than 70), covering 21.92% of the area.

The sloping land conversion program was piloted in some cities in 2000 and has been fully implemented since 2003. It is the largest conversion program with the feature of conversion of steep-slope or degraded cropland into forest or grassland [49,50]. The implementation of the program has greatly influenced the contribution of human activity.

Recent global evidence has demonstrated a direct human impact on global vegetation greening while the indirect drivers like climate change contributed about 40% [51]. However, the quantification of climate-driven and human-induced contribution results varies according to location, vegetation type, and target period [16,52,53]. Ge [54] have quantified the contribution to vegetation net primary productivity in China from 2001 to 2016, found the contribution of climate factors was about 60.06% and human activities contributed 39.94%. Moreover, it mentioned that climate change to vegetation dynamics was relatively lower in the Loess Plateau due to the sloping land conversion program.

Zheng [13] has taken the Loess Plateau as the study site, using NDVI as a proxy of grassland vegetation. The research found human activities contributed 42.35% to the vegetation change while climate change contributed 57.65%, which is consistent with our result. While Shi [55] revealed different results that climate change was responsible for 45.78% of NDVI variation while human activities were responsible for 54.22% in the Loess Plateau. The inconsistent result could be attributed to (1) different time periods of the dataset. Our study developed the data from 2000 to 2019, while Shi's covers 2000 to 2016. A new round of Grain for Green Project was implemented in Gansu Province during the year from 2014 to 2018, with 6.578 million hectares area restored to forests and grasslands (918,000 acres in Qingyang city). This could not be neglected during the analysis. (2) differs in satellite data. Our study used the MOD09 and MYD09 data with a spatial resolution of 250 m and temporal resolution of 0.5 days. While Shi's research utilized the MODIS NDVI dataset with a 1 km spatial resolution and a temporal resolution of 8 days. This might be led to the difference in quantitative contribution analysis.

### 3.5. FVC Response to ENSO and IOD Connections

The cross-correlation between the ONI and DMI indexes was calculated to further process the analysis on the effects of ENSO/IOD connections on the vegetation dynamics. The cross-correlation results of FVC against DMI (a and c) and ONI (b and d) are shown in Figure 12. For DMI, a unique result was identified, with a two-month (indicated by positive signs) spatial lag distribution. Some spots in the southwest, seem to precede DMI by three months (indicated by positive signs). The best correlations are located in the west of Huan county and the westernmost side of Huachi county. The lowest correlation was found in Ziwuling Forest. A more diverse result was apparent in the correlation against ONI. For the majority of the north, including Huan, Huachi, Qingcheng, and Heshui counties, a five-month lag (indicated by positive signs) was apparent. The remaining area excluding

the striped area of Ning, Zhengning, and Zhengyuan counties and Xifeng, appeared to precede ONI by 1–3 months. The shortest lag emerged in Zuwuling Forest, with a lag length of one month (indicating negative signs).

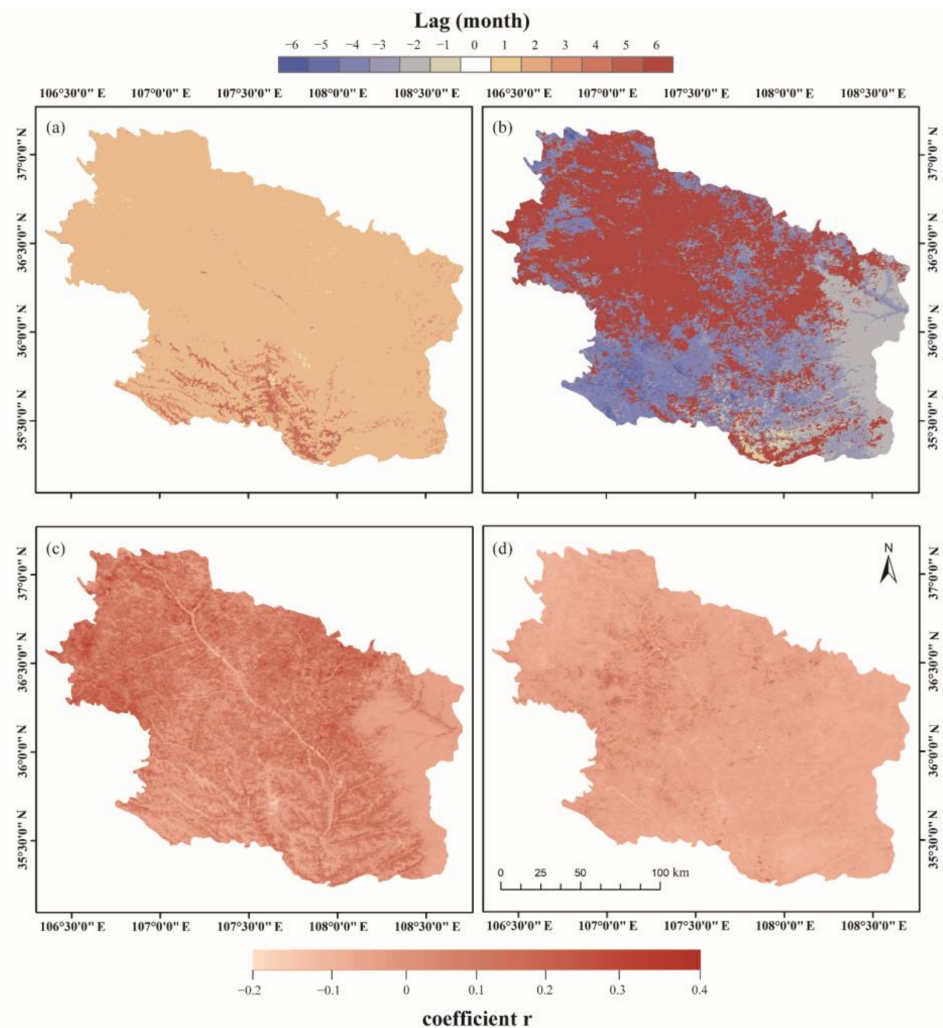


**Figure 12.** Cross-correlation results between FVC and DMI (a,c), ONI (b,d). The best time lags (a,b), and the corresponding correlation coefficients (b,d) were illustrated.

We identified a considerably strong dependence of FVC on DMI teleconnections (Figure 9) The vegetation response lagged by five months, but the associated linear relationship was considerably weaker compared to DMI. For the latter, there was a comparable time shift of up to three months (and more in the southwest part). In general, we concluded that supposed DMI has more influence on vegetation.

Coupled EI Nino/IOD+ stages had the most similar phase to the mean value while having a higher magnitude (Figure 13). For the growing season, a prolonged phase of maximum vegetation activity was identified in all EI Nino stages. Moreover, the minimum FVC value was observed under pure IOD+ stages. Moreover, for the following growing season, all groups gain a lower value compared to the mean, especially since June.

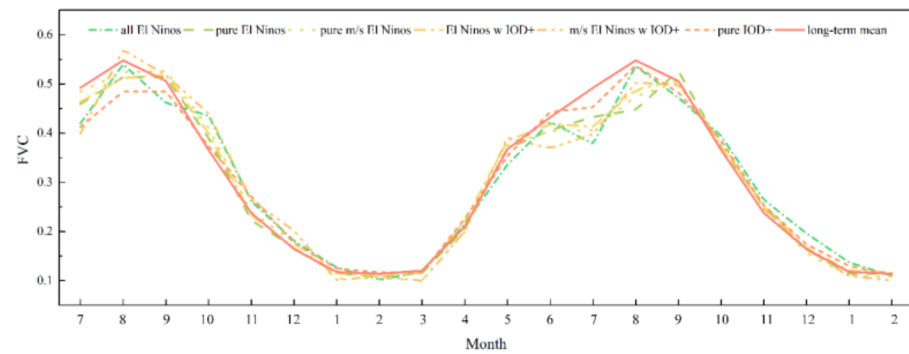


**Figure 13.** Average value of FVC in the study site during different El Niño/IOD+ stages from 2000 to 2019.

In contrast, coupled La Niña/IOD+ stages yielded below average FVC throughout the period, except for discrete months under some stages (Figure 14). This includes pure IOD+ in September and all La Niña stages in the next June. The pure La Niña and La Niña w IOD+ stage had a similar curve both in shape and magnitude. Unlike the ENSO stages, the prolonged phase was found in pure IOD+ stages. Compared to the ENSO stages, the curves of all groups were quite similar during the non-growing periods.

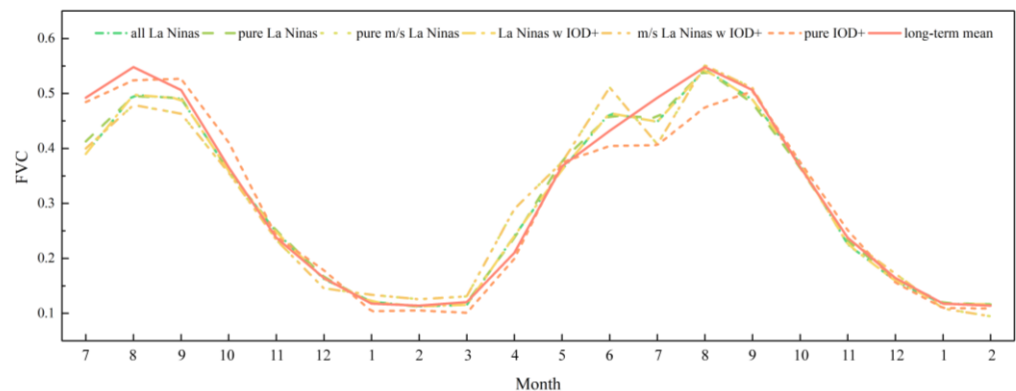


**Figure 14.** Average FVC value during La Niña/IOD+ periods from 2000 to 2019 in Qingyang city.

In general, there is a lag in climate change influences on vegetation growth, mostly more significant in the next growing season, both for ENSO and La Niña events.

### 3.6. Impact of Human Activity on FVC

Gansu province has experienced great modification by human activities in the recent two decades, especially with the implementation of the sloping land conversion program [56,57]. By deploying the MLR models, we separated the FVC trends dominated by climate factors and human activities.

To examine the possible influence of human activities in more detail, we factored in population and GDP data for the area (Figure 15). From 2011 to 2019, despite an increase in total population, Qingyang’s rural population declined as people migrated to the urban area. This could have contributed to lessening the pressure to encroach on naturally vegetated land, and further increasing FVC.

There was a good correlation between GDP demonstrated and FVC variation (Figure 16). Qingyang has implemented a grazing ban since 2010, and a subsidy and reward mechanism for grassland protection since 2011. As shown in Figure 11, Huan and Huachi counties were highly affected by human activity. These two counties have implemented a program to return grazing land to grassland, contributing a lot to the increasing trend of grassland and further to the FVC.

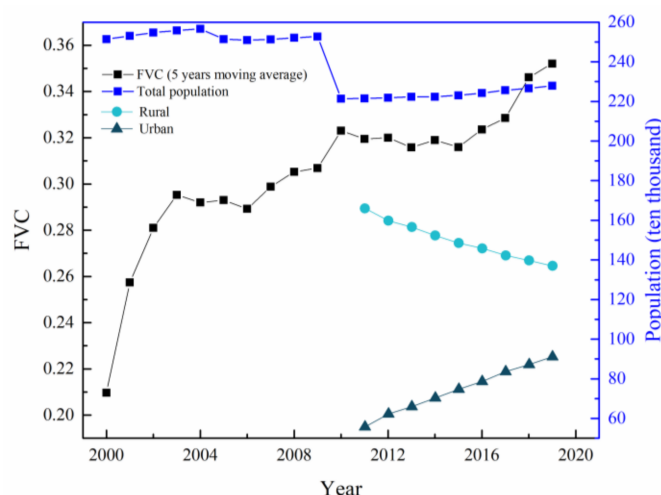


**Figure 15.** Relationship between population and FVC variation from 2000 to 2019 in Qingyang city.

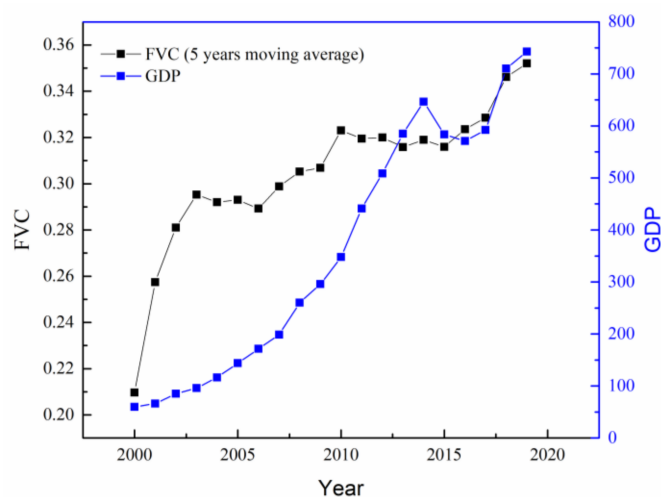


**Figure 16.** Relationship between FVC and GDP from 2000–2020 in Qingyang.

Also shown in Figure 16, the GDP of the primary industry has risen in the last two decades despite the implementation of the sloping land conversion program. This could be for three reasons. First, the higher FVC has effectively reduced land desertification and sand hazards. This further led to the most significant ecological change which is the reduction of the agricultural disaster areas and inundated areas. With improved agricultural production conditions, farming yields have been high and stable in recent decades. Second, agricultural products become more abundant since the start of the program. Through the program, cultivation on steep slopes and sandy areas with low and unstable grain yields but high ecological value was returned to vegetation, changing the long-standing practice of extensive planting and low yields. As a result, people pursued more intensive farming on land with better conditions. Third, the program freed up the rural labor force and enabled farmers to diversify into cultivating fruit and rearing livestock and providing other services, broadening the way to prosperity and rising incomes.

The five-year moving average of FVC was used in the analysis. A significant decrease was observed in 2010, while the FVC had a significant rise during this period. This demonstrated that the population tended to lessen the pressure to encroach on naturally vegetated land, and therefore could have contributed to the FVC increasing in the whole area. Another decreasing trend in population was identified in 2005 while no significant variation was found in FVC. This suggests that other variables had overwhelming influences on the vegetation changes.

#### 4. Conclusions

This study looked at the long-term temporal and spatial variation of FVC from 2000 to 2019 in Qingyang in Gansu province, a typical part of the Yellow River Basin. The area is ecologically fragile and a center for energy resources. We also explored the possible impacts of climatic and anthropogenic activities on FVC variation. The main conclusions relate to (1) the long-term spatial and temporal evolution of FVC trends for different administrative districts, (2) quantitative analysis of the influence of climatic factors and human activities on FVC change, and (3) the nonstationary response of FVC to the climate change factors.

Significant seasonal variation of vegetation was observed in Qingyang, with the maximum value in August. Significant latitudinal zonal distribution of vegetation was also observed throughout the whole year and the growing season, with an increasing trend from northwest to southeast.

In the past two decades, 96.71% of Qingyang showed an increasing trend of FVC with no obvious change in the FVC pattern. The annual average FVC was 30.71%, with the lowest value in 2000 (20.97%) and the highest value in 2018 (35.71%). Significant inter-annual changes were observed during the periods from 2000 to 2003, 2009 to 2010, and 2015 to 2019.

According to the time series decomposition results, five significant change points in trend components were revealed in July 2002, July 2003, August 2008, March 2012, and March 2018. Except for 2003 which had a decreasing trend, all periods showed an increasing trend. Significant irregular components appeared in 2012–2013 and 2015–2016, both of which were sudden increase points.

The MLR model indicated that FVC variation in Qingyang was led by a combination of climatic and human activity factors. In general, climate change contributed 54% and human activities 46%, respectively. In the area dominated by climatic factors, 98.73% exhibited an increasing trend. In the human activity-dominated area, 85.44% had an increasing trend. For the places with an increasing FVC trend, 55.89% of the area was dominated by human activity. For the area with a decreasing FVC trend, 75.42% of the area was impacted mainly by climatic factors.

By utilizing the ONI and DMI indexes, we explored the response of FVC to climate change (ENSO/IOD). Generally, the DMI index displayed a higher correlation compared to the ONI index, indicating that it had a more significant impact on vegetation growth in the study site. Spatial heterogeneity was observed in the lag month between the ONI index and FVC. Most of the area displayed 1–3 months in advance with two exceptions—the northern part of Qingyang (five months lag) and in Ziwuling forest (one month). Furthermore, the comparison between FVC and different ENSO/IOD and La Nina/IOD stages also proved the impact of climate change on vegetation growth, especially during the growing season for the following year.

**Author Contributions:** J.L. and G.W. conceptualization and methodology; J.Z.: review, discussion and suggestion to results; X.W. data curation, formal analysis and visualization. All authors have read and agreed to the published version of the manuscript.

**Funding:** The research was supported by the National Key Research and Development Programs of China (Grant No. 2021YFC3201100), the National Natural Science Foundation of China (Grant No.41901281), and the China Postdoctoral Science Foundation (Grant No. BX20190155).

**Institutional Review Board Statement:** Not applicable.

**Informed Consent Statement:** Not applicable.

**Data Availability Statement:** The data presented in this study are available on request from the corresponding author or the first author.

**Acknowledgments:** All authors do appreciate the journal editors and anonymous reviewers for their great efforts on the manuscript reviewing and constructive comments.

**Conflicts of Interest:** The authors declare no conflict of interest.

## References

1. Arowolo, A.O.; Deng, X.; Olatunji, O.A.; Obayelu, A.E. Assessing changes in the value of ecosystem services in response to land-use/land-cover dynamics in Nigeria. *Sci. Total Environ.* **2018**, *636*, 597–609. [\[CrossRef\]](#)
2. Rimal, B.; Sharma, R.; Kunwar, R.; Keshtkar, H.; Stork, N.E.; Rijal, S.; Rahman, S.A.; Baral, H. Effects of land use and land cover change on ecosystem services in the Koshi River Basin, Eastern Nepal. *Ecosyst. Serv.* **2019**, *38*, 100963. [\[CrossRef\]](#)
3. Li, X.; Chen, D.; Duan, Y.; Ji, H.; Zhang, L.; Chai, Q.; Hu, X. Understanding Land use/Land cover dynamics and impacts of human activities in the Mekong Delta over the last 40 years. *Glob. Ecol. Conserv.* **2020**, *22*, e00991. [\[CrossRef\]](#)
4. Huang, J.; Zhang, G.; Zhang, Y.; Guan, X.; Wei, Y.; Guo, R. Global desertification vulnerability to climate change and human activities. *Land Degrad. Dev.* **2020**, *31*, 1380–1391. [\[CrossRef\]](#)
5. Doelman, J.C.; Stehfest, E.; Tabeau, A.; van Meijl, H.; Lassaletta, L.; Gernaat, D.E.; Hermans, K.; Harmsen, M.; Daioglou, V.; Biemans, H. Exploring SSP land-use dynamics using the IMAGE model: Regional and gridded scenarios of land-use change and land-based climate change mitigation. *Glob. Environ. Chang.* **2018**, *48*, 119–135. [\[CrossRef\]](#)
6. Jia, K.; Liang, S.; Wei, X.; Yao, Y.; Yang, L.; Zhang, X.; Liu, D. Validation of Global Land Surface Satellite (GLASS) fractional vegetation cover product from MODIS data in an agricultural region. *Remote Sens. Lett.* **2018**, *9*, 847–856. [\[CrossRef\]](#)
7. Gitelson, A.A.; Kaufman, Y.J.; Stark, R.; Rundquist, D. Novel algorithms for remote estimation of vegetation fraction. *Remote Sens. Environ.* **2002**, *80*, 76–87. [\[CrossRef\]](#)
8. Jia, K.; Liang, S.; Gu, X.; Baret, F.; Wei, X.; Wang, X.; Yao, Y.; Yang, L.; Li, Y. Fractional vegetation cover estimation algorithm for Chinese GF-1 wide field view data. *Remote Sens. Environ.* **2016**, *177*, 184–191. [\[CrossRef\]](#)
9. Maliniemi, T.; Kapfer, J.; Saccone, P.; Skog, A.; Virtanen, R. Long-term vegetation changes of treeless heath communities in northern Fennoscandia: Links to climate change trends and reindeer grazing. *J. Veg. Sci.* **2018**, *29*, 469–479. [\[CrossRef\]](#)
10. Pan, N.; Feng, X.; Fu, B.; Wang, S.; Ji, F.; Pan, S. Increasing global vegetation browning hidden in overall vegetation greening: Insights from time-varying trends. *Remote Sens. Environ.* **2018**, *214*, 59–72. [\[CrossRef\]](#)
11. Gondhalekar, D.; Ramsauer, T. Nexus city: Operationalizing the urban water-energy-food nexus for climate change adaptation in Munich, Germany. *Urban Clim.* **2017**, *19*, 28–40. [\[CrossRef\]](#)
12. Ghadge, A.; Wurtmann, H.; Seuring, S. Managing climate change risks in global supply chains: A review and research agenda. *Int. J. Prod. Res.* **2020**, *58*, 44–64. [\[CrossRef\]](#)
13. Zheng, K.; Wei, J.-Z.; Pei, J.-Y.; Cheng, H.; Zhang, X.-L.; Huang, F.-Q.; Li, F.-M.; Ye, J.-S. Impacts of climate change and human activities on grassland vegetation variation in the Chinese Loess Plateau. *Sci. Total Environ.* **2019**, *660*, 236–244. [\[CrossRef\]](#)
14. Qu, S.; Wang, L.; Lin, A.; Zhu, H.; Yuan, M. What drives the vegetation restoration in Yangtze River basin, China: Climate change or anthropogenic factors? *Ecol. Indic.* **2018**, *90*, 438–450. [\[CrossRef\]](#)
15. Mahmoud, S.H.; Gan, T.Y. Impact of anthropogenic climate change and human activities on environment and ecosystem services in arid regions. *Sci. Total Environ.* **2018**, *633*, 1329–1344. [\[CrossRef\]](#)
16. Qi, X.; Jia, J.; Liu, H.; Lin, Z. Relative importance of climate change and human activities for vegetation changes on China's silk road economic belt over multiple timescales. *Catena* **2019**, *180*, 224–237. [\[CrossRef\]](#)
17. Zheng, K.; Tan, L.; Sun, Y.; Wu, Y.; Duan, Z.; Xu, Y.; Gao, C. Impacts of climate change and anthropogenic activities on vegetation change: Evidence from typical areas in China. *Ecol. Indic.* **2021**, *126*, 107648. [\[CrossRef\]](#)
18. Peng, S.; Gang, C.; Cao, Y.; Chen, Y. Assessment of climate change trends over the Loess Plateau in China from 1901 to 2100. *Int. J. Climatol.* **2018**, *38*, 2250–2264. [\[CrossRef\]](#)
19. Jia, K.; Yang, L.; Liang, S.; Xiao, Z.; Zhao, X.; Yao, Y.; Zhang, X.; Jiang, B.; Liu, D. Long-term Global Land Surface Satellite (GLASS) fractional vegetation cover product derived from MODIS and AVHRR Data. *IEEE J. Sel. Top. Appl. Earth Obs. Remote Sens.* **2018**, *12*, 508–518. [\[CrossRef\]](#)
20. Jia, K.; Liang, S.; Liu, S.; Li, Y.; Xiao, Z.; Yao, Y.; Jiang, B.; Zhao, X.; Wang, X.; Xu, S. Global land surface fractional vegetation cover estimation using general regression neural networks from MODIS surface reflectance. *IEEE Trans. Geosci. Remote Sens.* **2015**, *53*, 4787–4796. [\[CrossRef\]](#)
21. Baret, F.; Hagolle, O.; Geiger, B.; Bicheron, P.; Miras, B.; Huc, M.; Berthelot, B.; Niño, F.; Weiss, M.; Samain, O. LAI, fAPAR and fCover CYCLOPES global products derived from VEGETATION: Part 1: Principles of the algorithm. *Remote Sens. Environ.* **2007**, *110*, 275–286. [\[CrossRef\]](#)
22. Baret, F.; Pavageau, K.; Béal, D.; Weiss, M.; Berthelot, B.; Regner, P. *Algorithm Theoretical Basis Document for MERIS Top of Atmosphere Land Products (TOA\_VEG)*; INRA-CSE: Avignon, France, 2006.
23. Yang, L.; Jia, K.; Liang, S.; Liu, J.; Wang, X. Comparison of four machine learning methods for generating the GLASS fractional vegetation cover product from MODIS data. *Remote Sens.* **2016**, *8*, 682. [\[CrossRef\]](#)
24. Lu, C.; Pang, M.; Yang, J.; Wang, D. Research on interactions between the economy and environment in tourism development: Case of Qingyang, China. *Sustainability* **2018**, *10*, 4033. [\[CrossRef\]](#)
25. Wu, Y.; Zhang, N.; Wang, Y.; Ren, Y.; Yuan, Z.; Li, N. Concentrations of polycyclic aromatic hydrocarbons in street dust from bus stops in Qingyang city: Estimates of lifetime cancer risk and sources of exposure for daily commuters in Northwest China. *Environ. Pollut.* **2020**, *266*, 115222. [\[CrossRef\]](#)
26. Liu, L.; Liang, Y.; Hashimoto, S. Integrated assessment of land-use/coverage changes and their impacts on ecosystem services in Gansu Province, northwest China: Implications for sustainable development goals. *Sustain. Sci.* **2020**, *15*, 297–314. [\[CrossRef\]](#)

27. Vermote, E.F.; El Saleous, N.Z.; Justice, C.O. Atmospheric correction of MODIS data in the visible to middle infrared: First results. *Remote Sens. Environ.* **2002**, *83*, 97–111. [[CrossRef](#)]
28. Hou, A.Y.; Kakar, R.K.; Neeck, S.; Azarbarzin, A.A.; Kummerow, C.D.; Kojima, M.; Oki, R.; Nakamura, K.; Iguchi, T. The global precipitation measurement mission. *Bull. Am. Meteorol. Soc.* **2014**, *95*, 701–722. [[CrossRef](#)]
29. Baniya, B.; Tang, Q.; Huang, Z.; Sun, S.; Techato, K.-a. Spatial and temporal variation of NDVI in response to climate change and the implication for carbon dynamics in Nepal. *Forests* **2018**, *9*, 329. [[CrossRef](#)]
30. Lou, J.; Xu, G.; Wang, Z.; Yang, Z.; Ni, S. Multi-Year NDVI Values as Indicator of the Relationship between Spatiotemporal Vegetation Dynamics and Environmental Factors in the Qaidam Basin, China. *Remote Sens.* **2021**, *13*, 1240. [[CrossRef](#)]
31. Maneja, R.H.; Miller, J.D.; Li, W.; El-Askary, H.; Flandez, A.V.B.; Dagoy, J.J.; Alcaria, J.F.A.; Basali, A.U.; Al-Abdulkader, K.A.; Loughland, R.A. Long-term NDVI and recent vegetation cover profiles of major offshore island nesting sites of sea turtles in Saudi waters of the northern Arabian Gulf. *Ecol. Indic.* **2020**, *117*, 106612. [[CrossRef](#)]
32. Tucker, C.J. Red and photographic infrared linear combinations for monitoring vegetation. *Remote Sens. Environ.* **1979**, *8*, 127–150. [[CrossRef](#)]
33. Brown, M.E.; Pinzón, J.E.; Didan, K.; Morisette, J.T.; Tucker, C.J. Evaluation of the consistency of long-term NDVI time series derived from AVHRR, SPOT-vegetation, SeaWiFS, MODIS, and Landsat ETM+ sensors. *IEEE Trans. Geosci. Remote Sens.* **2006**, *44*, 1787–1793. [[CrossRef](#)]
34. Wang, Y.; Liu, Y.; Jin, J. Contrast effects of vegetation cover change on evapotranspiration during a revegetation period in the Poyang Lake Basin, China. *Forests* **2018**, *9*, 217. [[CrossRef](#)]
35. Gong, Z.; Zhao, S.; Gu, J. Correlation analysis between vegetation coverage and climate drought conditions in North China during 2001–2013. *J. Geogr. Sci.* **2017**, *27*, 143–160. [[CrossRef](#)]
36. Zhao, J.; Li, J.; Liu, Q.; Xu, B.; Yu, W.; Lin, S.; Hu, Z. Estimating fractional vegetation cover from leaf area index and clumping index based on the gap probability theory. *Int. J. Appl. Earth Obs. Geoinf.* **2020**, *90*, 102112. [[CrossRef](#)]
37. Montandon, L.; Small, E. The impact of soil reflectance on the quantification of the green vegetation fraction from NDVI. *Remote Sens. Environ.* **2008**, *112*, 1835–1845. [[CrossRef](#)]
38. Li, J.; Ma, R.; Xue, K.; Loisel, S. Drivers to spatial and temporal dynamics of column integrated phytoplankton biomass in the shallow lake of Chaohu, China. *Ecol. Indic.* **2020**, *109*, 105812. [[CrossRef](#)]
39. Loisel, H.; Vantrepotte, V.; Ouillon, S.; Ngoc, D.D.; Herrmann, M.; Tran, V.; Mériaux, X.; Dessailly, D.; Jamet, C.; Duhaut, T. Assessment and analysis of the chlorophyll-a concentration variability over the Vietnamese coastal waters from the MERIS ocean color sensor (2002–2012). *Remote Sens. Environ.* **2017**, *190*, 217–232. [[CrossRef](#)]
40. Henderson, R. Note on graduation by adjusted average. *Trans. Actuar. Soc. Am.* **1916**, *17*, 43–48.
41. Vantrepotte, V.; Mélin, F. Temporal variability of 10-year global SeaWiFS time-series of phytoplankton chlorophyll a concentration. *ICES J. Mar. Sci.* **2009**, *66*, 1547–1556. [[CrossRef](#)]
42. Pezzulli, S.; Stephenson, D.; Hannachi, A. The variability of seasonality. *J. Clim.* **2005**, *18*, 71–88. [[CrossRef](#)]
43. Chan, K.-S.; Ripley, B. TSA: Time series analysis. *R Package Version* **2012**, *1*, 22–1821.
44. Hilker, T.; Natsagdorj, E.; Waring, R.H.; Lyapustin, A.; Wang, Y. Satellite observed widespread decline in Mongolian grasslands largely due to overgrazing. *Glob. Chang. Biol.* **2014**, *20*, 418–428. [[CrossRef](#)]
45. Mao, D.; Wang, Z.; Wu, B.; Zeng, Y.; Luo, L.; Zhang, B. Land degradation and restoration in the arid and semiarid zones of China: Quantified evidence and implications from satellites. *Land Degrad. Dev.* **2018**, *29*, 3841–3851. [[CrossRef](#)]
46. Wang, B.; Gao, P.; Niu, X.; Sun, J. Policy-driven China's Grain to Green Program: Implications for ecosystem services. *Ecosyst. Serv.* **2017**, *27*, 38–47. [[CrossRef](#)]
47. Wessels, K.J.; Van Den Bergh, F.; Scholes, R. Limits to detectability of land degradation by trend analysis of vegetation index data. *Remote Sens. Environ.* **2012**, *125*, 10–22. [[CrossRef](#)]
48. Chun, X.; Yong, M.; Liu, J.; Liang, W. Monitoring land cover change and its dynamic mechanism on the Qehan Lake Basin, Inner Mongolia, North China, during 1977–2013. *Environ. Monit. Assess.* **2018**, *190*, 1–17. [[CrossRef](#)]
49. Dang, X.; Gao, S.; Tao, R.; Liu, G.; Xia, Z.; Fan, L.; Bi, W. Do environmental conservation programs contribute to sustainable livelihoods? Evidence from China's grain-for-green program in northern Shaanxi province. *Sci. Total Environ.* **2020**, *719*, 137436. [[CrossRef](#)]
50. Hu, Y.; Zhen, L.; Zhuang, D. Assessment of land-use and land-cover change in Guangxi, China. *Sci. Rep.* **2019**, *9*, 1–13. [[CrossRef](#)]
51. Song, X.-P.; Hansen, M.C.; Stehman, S.V.; Potapov, P.V.; Tyukavina, A.; Vermote, E.F.; Townshend, J.R. Global land change from 1982 to 2016. *Nature* **2018**, *560*, 639–643. [[CrossRef](#)]
52. Huang, S.; Kong, J. Assessing land degradation dynamics and distinguishing human-induced changes from climate factors in the Three-North Shelter forest region of China. *ISPRS Int. J. Geo-Inf.* **2016**, *5*, 158. [[CrossRef](#)]
53. Li, Q.; Zhang, C.; Shen, Y.; Jia, W.; Li, J. Quantitative assessment of the relative roles of climate change and human activities in desertification processes on the Qinghai-Tibet Plateau based on net primary productivity. *Catena* **2016**, *147*, 789–796. [[CrossRef](#)]
54. Ge, W.; Deng, L.; Wang, F.; Han, J. Quantifying the contributions of human activities and climate change to vegetation net primary productivity dynamics in China from 2001 to 2016. *Sci. Total Environ.* **2021**, *773*, 145648. [[CrossRef](#)] [[PubMed](#)]
55. Shi, S.; Yu, J.; Wang, F.; Wang, P.; Zhang, Y.; Jin, K. Quantitative contributions of climate change and human activities to vegetation changes over multiple time scales on the Loess Plateau. *Sci. Total Environ.* **2021**, *755*, 142419. [[CrossRef](#)] [[PubMed](#)]

- 
56. Lu, G.; Yin, R. Evaluating the Evaluated Socioeconomic Impacts of China's Sloping Land Conversion Program. *Ecol. Econ.* **2020**, *177*, 106785. [[CrossRef](#)]
  57. Li, L.; Liu, C.; Liu, J.; Cheng, B. Has the Sloping Land Conversion Program in China impacted the income and employment of rural households? *Land Use Policy* **2021**, *109*, 105648. [[CrossRef](#)]